

Ultrabroadband and Multifunctional Achromatic Mikaelian Lens on an Elastic Plate


Jin Chen^{1,2}, Guangyuan Su,³ Shaohang Xu,³ Mingji Chen^{2,*}, Yongquan Liu,^{3,†} Daining Fang,^{2,‡} and Ji Zhou⁴

¹*School of Optical and Electronic Information, Huazhong University of Science and Technology, Wuhan 430074, China*

²*Institute of Advanced Structure Technology, Beijing Institute of Technology, Beijing 100081, China*

³*State Key Laboratory for Strength and Vibration of Mechanical Structures, Department of Engineering Mechanics, School of Aerospace Engineering, Xi'an Jiaotong University, Xi'an 710049, China*

⁴*State Key Laboratory of New Ceramics and Fine Processing, School of Materials Science and Engineering, Tsinghua University, Beijing 100084, China*

 (Received 12 July 2022; revised 3 August 2022; accepted 1 September 2022; published 15 December 2022)

The emergence and development of acoustic artificial materials stimulate a large number of applications for the manipulation of ultrasonic and elastic waves. Most of the reported metasurfaces and metamaterials only work effectively at a given frequency and target a fixed functionality. Reconfigurable designs may solve this problem, to a certain extent, but require the introduction of complex active control components. Here, by integrating multiple functionalities on a conformally mapped Mikaelian lens with a hyperbolic secant refractive-index distribution, a broadband passive lens is presented and accomplished on an elastic plate. Just by adjusting the location and type of source, different regulations of flexural waves can be switched from one sort to another. Through projecting the refractive-index profile onto the thickness of the plates, the proposed Mikaelian lens is designed and fabricated. Theoretical prediction and experimental results demonstrate beam scanning at an angle of up to 120° from 30 to 180 kHz and achromatic subwavelength focusing with a full width at half maximum of around 0.3λ from 30 to 120 kHz. Without using locally resonant materials or active control elements, this work provides a feasible way to construct multifunctional flexural-wave devices.

DOI: [10.1103/PhysRevApplied.18.064047](https://doi.org/10.1103/PhysRevApplied.18.064047)

I. INTRODUCTION

Metamaterials have been developed rapidly owing to their artificially regulated physical characteristics, which significantly strengthen the flexibility to manipulate wave fields. As theoretical support, transformation optics [1,2] then provided a paradigm to control electromagnetic waves or light rays utilizing metamaterials. A great many optical devices, such as cloaks [3–5], concentrators [6–8], and perfect lenses [9–11], were successfully designed and verified. Subsequently, the transformation method was extended to acoustics and elastic waves [12–20], surface-water waves [21], and even matter waves [22]. However, the realization of a metamaterial is generally a big challenge due to its complex microstructure and bulky configuration. Therefore, the focus gradually turns to a metasurface, which is the lower-dimensional version of a metamaterial, for its

compact form and easy fabrication. By gradual cumulative phase variation along the metasurface, the wave front can be modulated based on the generalized Snell law [23]. A huge number of devices, such as beam scanning and focusing [24–26], carpet cloaking [27], optical or acoustic holograms [28], and perfect absorption or insulation [29,30], have been achieved accordingly.

Although great success has been achieved in metamaterials and metasurfaces, they are still far from being suitable for real applications, because most existing metamaterials are restricted by their solidified function in a narrow frequency range or even at a fixed frequency. Programmable and reconfigurable metamaterials [31–34] were presented and developed to solve this problem. By using active or mechanically reconfigurable elements, multiple functionalities are also realized under different circumstances. For example, using external loadings, a unit cell's mechanical instability is utilized to implement function switching [32]. Memoli *et al.* [35] proposed another creative way to scan an acoustic beam for different angles by reassembling predesigned metamaterial bricks. Most recently, by adjusting the height of the water surface in the cavity of

*mjchen81@bit.edu.cn

†liuy2018@xjtu.edu.cn

‡fangdn@bit.edu.cn

each unit cell independently [36], the phase change generated by each unit cell can be tuned continuously. Tunability is also achieved by piezoelectric materials [37]. Furthermore, the real-time tunability is confirmed by using a complex feedback control system [38].

In the technological paths mentioned above, the physical properties of each unit cell must be changeable under external stimuli, which is complex and costly for practical applications of on-chip acoustic or elastic wave devices. To overcome this issue, an alternative way, identified as the multiplexing technique [28], is proposed in optics to achieve multifunctional devices. Just by changing the polarization, frequencies, or amplitudes of incident waves, the performed functions can be switched from one to another. A variety of devices, such as angle-sensitive [39], frequency-sensitive [40], polarization-sensitive [41], helicity-sensitive [42], and multiplexed metasurfaces, were realized in recent years. For acoustic or elastic waves, an amplitude-multiplexed acoustic topological insulator [43] and a frequency-multiplexed elastic metasurface [44] with beam-steering and -focusing functions have been accomplished. However, the realization of passive multifunctional elastic devices over a broadband frequency range remains a big challenge.

Under the assumption of Kirchoff-Love (KL) thin-plate theory [45], the conformal-transformation [46] method is applied in this work. Inspired by the conformally mapped

Mikaelian lens in optics [47,48] and acoustics [49], a broadband passive multifunctional Mikaelian lens for flexural waves is presented. In contrast to highly dispersive and anisotropic metamaterials, the gradient-refractive-index (GRIN) profile of the lens is achieved by gradually adjusting the thickness of the plate. Just by adjusting the location and type of source, we numerically and experimentally achieve beam scanning up to 120° from 30 to 180 kHz and achromatic subwavelength focusing with a full width at half maximum (FWHM) of about 0.3λ from 30 to 120 kHz. This work provides a feasible way to design broadband and multifunctional devices for guided elastic waves.

II. THEORETICAL DESIGN OF CONFORMALLY MAPPED MIKAEELIAN LENS FOR FLEXURAL WAVES

First, we study a Maxwell fish-eye lens. The Maxwell fish-eye lens can transport information from a point source located at the edge of the lens to the exact opposite side. For the two-dimensional (2D) case in Fig. 1(a), its refractive-index profile is described as $2\alpha/(1+r^2)$, where α and r represent the refractive index on the boundary of the lens and the distance from the center of the lens, respectively. Ray paths indicate that light released from point A will travel along the circles and merge into an

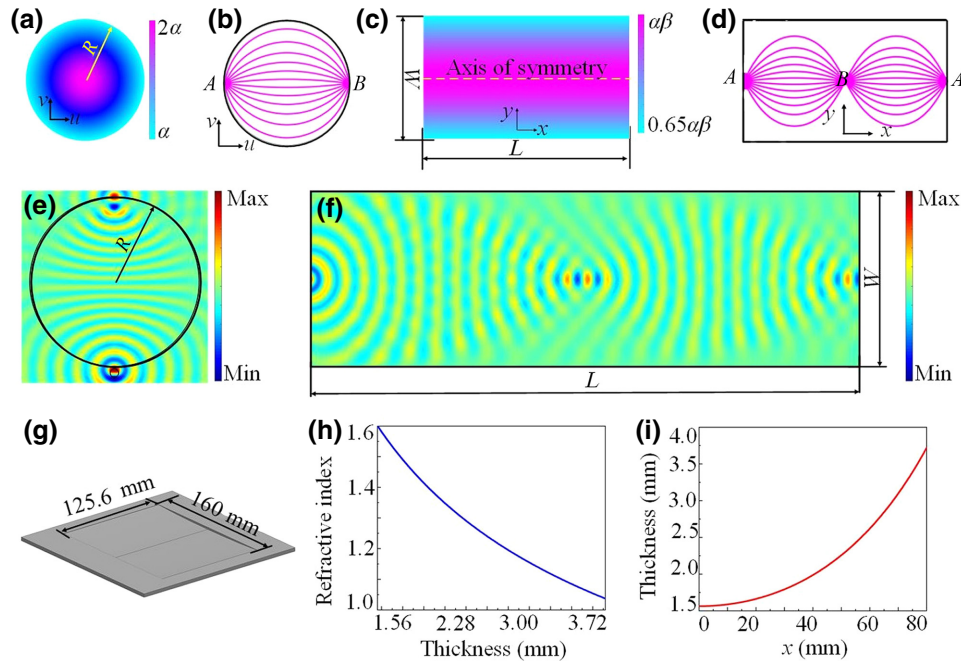


FIG. 1. Theoretical design of passive multifunctional flexural-wave Mikaelian lens via conformal transformation. (a) Refractive-index distribution of Maxwell fish-eye lens. (b),(e) Imaging performance of Maxwell fish-eye lens in u - v space. (c) Refractive index of mapped Mikaelian lens. (d),(f) Self-focusing phenomenon of Mikaelian lens in x - y space. (g) Three-dimensional model of conformally mapped Mikaelian lens to collimated flexural waves. (h) Relationship between the effective refraction index of the plate and the thickness. (i) Connection between thickness and the distance from the center of the lens.

image at point B , as revealed in Fig. 1(b). This imaging performance is also verified by the wave-field distribution in Fig. 1(e). Then, the principle of the conformal-transformation method (COM) is first reviewed [50]. For 2D space explained by $w = u + iv$ with a refractive-index distribution of $n_w(u + iv)$, incident waves propagating through this 2D space will travel along a curved path. Another 2D space described by $z = x + iy$ can be linked to the former one by conformal mapping, $w = w(z)$, which meets the requirement of the Cauchy-Riemann condition [51]. Therefore, the relationship between u - v and x - y space is finally established. The corresponding refractive-index distribution in x - y space is derived as follows [50]:

$$n_z = n_w |d_w/d_z|, \quad (1)$$

in which n_z and n_w are the refractive-index profile in the z space and w space, respectively. d_z and d_w are distance microelements in the z space and w space, respectively. By exerting an exponential conformal transformation $w(\mu, \nu) = e^{\beta z(x, y)}$ on Maxwell fish-eye lens in virtual space, the resulting refractive-index profile in physical space will be transformed into

$$n_z(x, y) = n_0 \operatorname{sech}(\beta x), \quad (2)$$

which is identical to a Mikaelian lens' refractive-index distribution, where β denotes the coefficient that governs the length of the mapped region by $l = 2\pi/\beta$, $n_0 = \alpha\beta$ is the maximum refractive index along the central line, and α and β are regularly defined as one. When the radius of the Maxwell fish-eye lens is restricted to R , then the mapped region of the Mikaelian lens is a rectangle with a width of $W = 2R$ and length of $L = 2\pi R/\beta$. The related refractive-index profile is described in Fig. 1(c), which clearly illustrates a gradual increase of the refractive index from the edge at both sides towards the axis of symmetry of the lens. Through transforming ray tracing in Fig. 1(b) by $w(\mu, \nu) = e^{\beta z(x, y)}$, a sinelike path and self-focusing phenomenon is observed inside the Mikaelian lens, as depicted in Fig. 1(d), which can also be derived by the variational method of geometric optics. The corresponding wave-field pattern given by Fig. 1(f) further confirms the Mikaelian lens' capability of self-focusing. To obtain the ultrawide-angle beam scanning and achromatic subwavelength GRIN lens over a broadband frequency range, first the conformally mapped Mikaelian lens is truncated to a quarter; the length of the new version of the Mikaelian lens decreases to $\pi R/(2\beta)$. Second, the value of α is adjusted to 1.6 to guarantee a broadband operating-frequency range.

The designed Mikaelian lens is embedded on a thin aluminium plate with a Young's modulus of 70 GPa, Poisson's ratio of 0.33, and mass density of 2700 kg/m³ by varying the thickness, as shown in Fig. 1(g). The thickness of the host plate, h_0 , is selected to be 4 mm with dimensions of 180 × 180 mm². The effective refraction index,

$n(x, y)$, of the plate is controlled by the local thickness, $h(x, y)$ [52], according to

$$n(x, y) = \sqrt{\frac{h_0}{h(x, y)}}. \quad (3)$$

The corresponding relationship between the effective refraction index of the plate and the thickness is illustrated in Fig. 1(h). The thickness as a function of the distance from the center of the lens is plotted in Fig. 1(i). It can be observed that a striking value of $n = 1.6$ is accomplished at the center of the lens through a relatively high thickness (1.5625 mm), which implies that the flexural wave can experience a significant refraction without introducing a very thin truncation thickness.

For the analytical analysis of flexural-wave propagation inside the 2D conformally mapped Mikaelian lens, we adopt the geometrical acoustics approximation (GAA) [53,54]. A relatively simple analysis of a flexural wave traveling in the GRIN medium on thin plates is provided by the GAA. Through calculating the ray trajectory of point sources located at different positions at the back surface of our designed Mikaelian lens, it is found that highly directional plane waves propagating in different directions are generated. Figures 2(a)–2(d) illustrate the related ray trajectories of point sources placed at $x = 0$ mm, $x = 30$ mm, $x = 60$ mm, and $x = 80$ mm. It can be clearly observed that, with the point source moving towards the edge of the lens, the deflection angle increases from 0° to 60°. Owing to the symmetry of the designed Mikaelian lens, for the point source placed in the negative direction, the same trend of deflection angle can be predicted and yielded.

III. SIMULATED RESULTS AND ANALYSIS OF MIKAELIAN LENS

To investigate the performance of the conformally mapped Mikaelian lens comprehensively, the full-wave numerical simulation is adopted and carried out using the commercial software COMSOL Multiphysics 5.5. For the point source placed at four different places at a frequency of 120 kHz, the results of simulated displacement-field patterns are given in Figs. 2(e)–2(h), which are highly consistent with the calculated ray trajectories shown in Figs. 2(a)–2(d). The deflection angle of the transmitted flexural wave with a point source located at the center of the Mikaelian lens is defined as 0°, which is also the reference of the deflection angle generated by other point sources. Thus, it can be seen that, as the point source advances toward the edge of the lens, the deflection angle of the outgoing beam gradually increases to 60°. Our proposed lens' ability to yield a highly directional emission within a viewing angle of 120° is fully confirmed. Thereafter, to demonstrate the broadband property of our designed

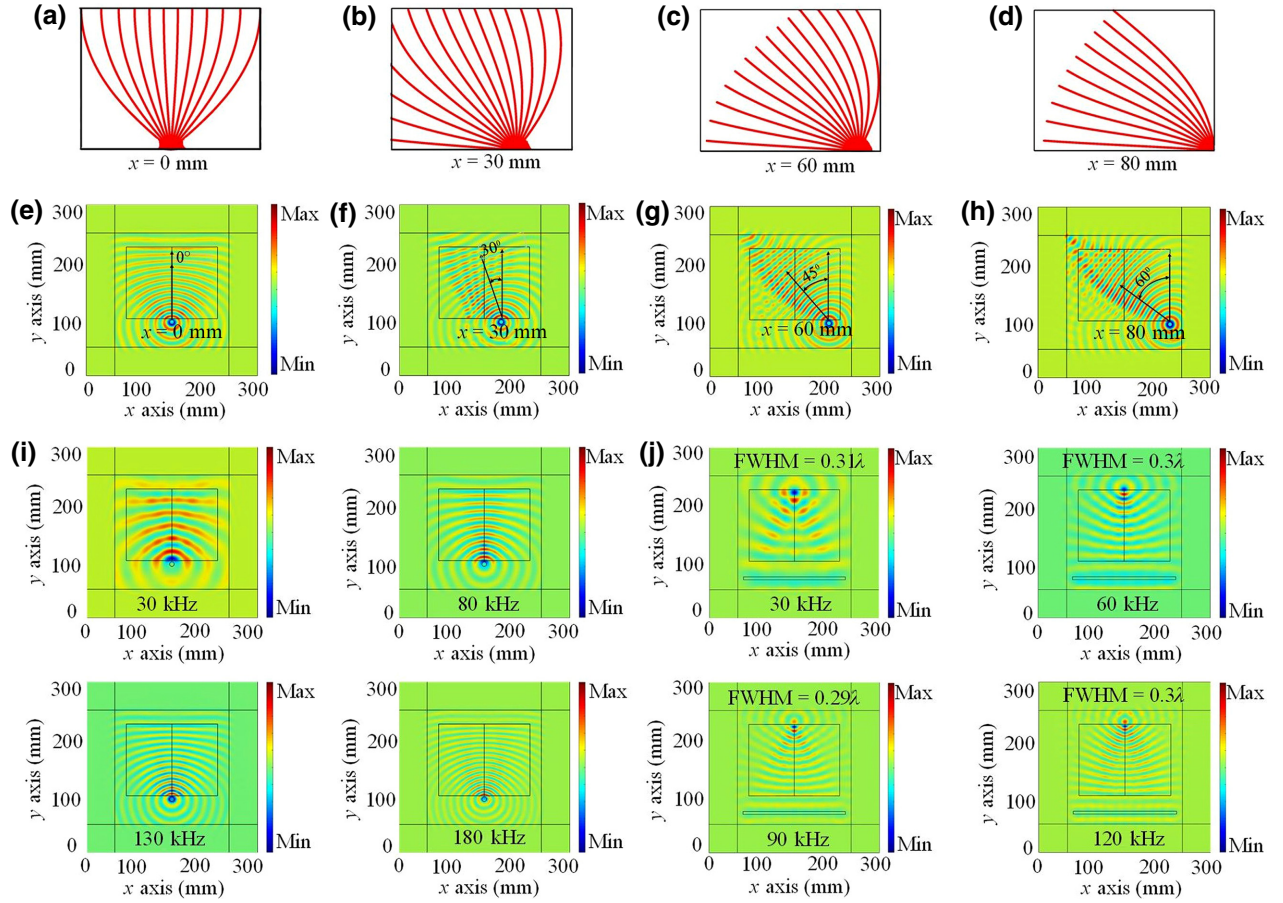


FIG. 2. Simulated performance of passive multifunctional flexural-wave Mikaelian lens. (a)–(d) Calculated ray trajectories for point sources located at $x = 0$ mm, $x = 30$ mm, $x = 60$ mm, and $x = 80$ mm. (e)–(h) Related displacement-field patterns of beam scanning at a frequency of 120 kHz. (i) Broadband beam collimation performance from 30 to 180 kHz. (j) Displacement-field distributions for broadband achromatic subwavelength focusing from 30 to 120 kHz.

Mikaelian lens, the vertical-displacement-field distribution from 30 to 180 kHz of a point source located at the center the lens is simulated and plotted in Fig. 2(i). It is obvious that highly directional quasiplane waves are produced in this wide frequency range. The broadband characteristic of our proposed lens to control the propagation of a flexural wave is validated, indicating that our design method is effective. According to the reciprocal principle, achromatic focusing can also be achieved, as long as our proposed lens is illuminated by plane waves. Figure 2(j) illustrates the corresponding simulated displacement-field patterns from 30 to 120 kHz. Achromatic subwavelength focusing can be clearly observed. The related FWHM varies from 0.29λ to 0.31λ . Since the refractive index at the focusing point is 1.6, according to the diffraction limit the derived FWHM is reasonable. This property has great potential to be applied in energy harvesting and medical imaging in the future. It can be concluded that our design is fully verified numerically.

IV. EXPERIMENTAL RESULTS AND DISCUSSION

To further prove the high performance, an experimental setup is established, as exhibited in Fig. 3, to complete the verification of ultrawide-angle beam scanning and broadband achromatic subdiffraction focusing. Our designed flexural-wave Mikaelian lens is manufactured by Computer Numerical Control Machining. The three-cycle tone burst, $F(t) = [1 - \cos(2\pi f_c t/3)]\sin(2\pi f_c t)$, with $f_c = 45$ kHz being the central frequency, is exerted by a RIGOL DG4062 wave generator as the signal source. To enhance the signal-to-noise ratio, a power amplifier is used to magnify the three-cycle tone burst. Piezoelectric patches ignited by the power amplifier are bonded to fabricated plates with adhesive for excitation. A Polytec NLV-2500 laser vibrometer installed at the two-axis motorized stage is the receiving probe to measure the amplitude and phase of the out-of-plane displacement field. As the two-axis motorized stage moves step by step, data of transmitted out-of-plane displacement fields are obtained and stored on

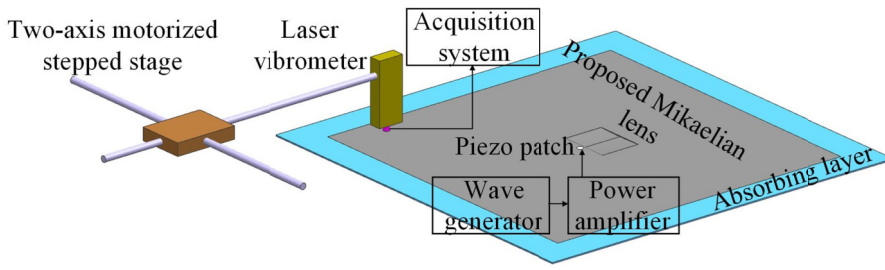


FIG. 3. Experimental setup for measuring the vertical-displacement-field distribution.

a computer via an oscilloscope (PicoScope 4000 series). Then, through fast Fourier transform, postprocessing data are consistent with monochromatic theory. The corresponding scanning zone is $200 \times 170 \text{ mm}^2$. Furthermore, the wave fields of neighboring frequencies can also be investigated by our input signal. Therefore, the wave fields of the broadband frequency range can be gained by only one measurement. To guarantee the precision of the experiment, an absorbing layer is added to the fabricated plate. The capability of the proposed Mikaelian lens to accomplish ultrawide-angle beam scanning is first tested. Five circular piezoelectric patches ($r = 10 \text{ mm}$) are bonded to the fabricated plate at the edge of the Mikaelian lens to be used as point sources. From Fig. 4(a), it can be seen that the coordinates of these five piezoelectric patches on the x axis are $0, -30, 30, -60,$ and 60 mm , which are in accordance with our simulation. Moreover, these five piezoelectric patches are excited independently to ensure that different

deflection angles at different places can be checked individually. Measured results of the vertical-displacement-field distribution and corresponding deflection angles at a frequency of 60 kHz for the five point sources located in different places are depicted in Figs. 4(b)–4(f). Comparing Figs. 4(b)–4(f) with Figs. 2(e)–2(h), it is obvious that the measured deflection angles are highly consistent with the theoretical ones. There is no doubt that the beam-scanning function of the proposed Mikaelian lens is proved.

For the measurement of broadband achromatic sub-wavelength focusing, an array of six square piezoelectric patches ($40 \times 12 \text{ mm}^2$) are bonded to the fabricated plate to generate a normally incident plane wave approximately and are 150 mm away from the Mikaelian lens, as plotted in Fig. 4(g). From the measured vertical-displacement-field patterns from 30 to 60 kHz , depicted in Figs. 4(h)–4(k), and the corresponding FWHM given

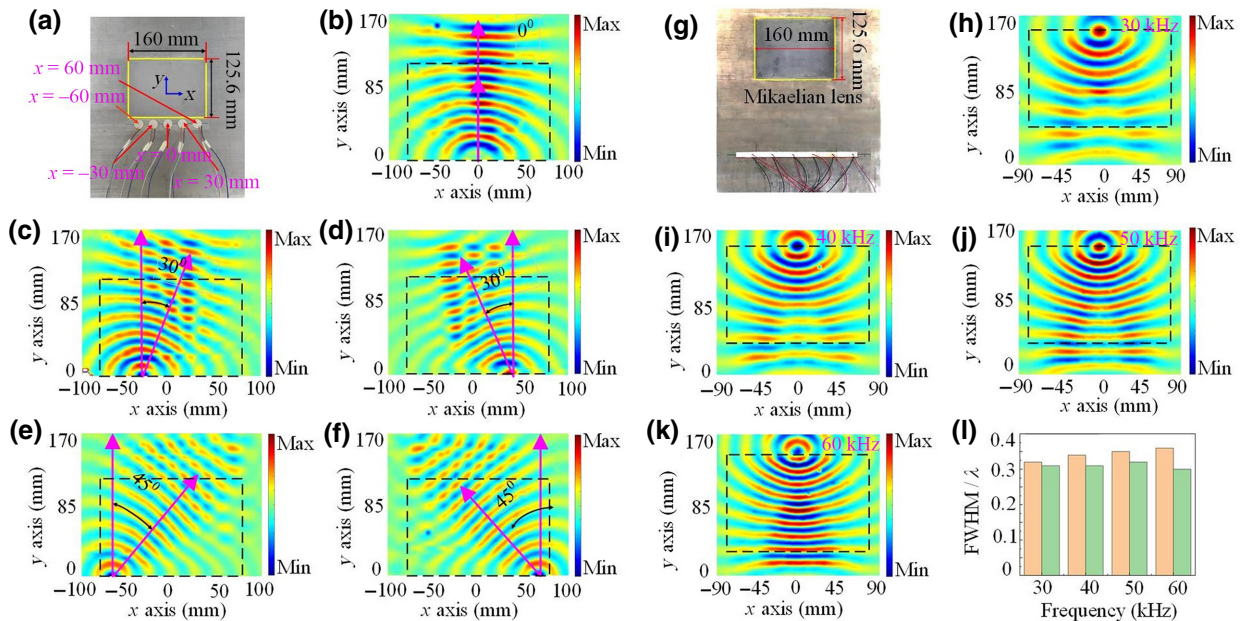


FIG. 4. Experimental verification of passive multifunctional flexural-wave Mikaelian lens. (a) Photograph of flexural-wave Mikaelian lens with five point sources. (b)–(f) Measured displacement-field distribution and related deflection angle at a frequency of 60 kHz when point sources are placed at $x = 0 \text{ mm}, \pm 30 \text{ mm},$ and $\pm 60 \text{ mm}$; black dashed line represents the Mikaelian lens. (g) Photograph of fabricated flexural-wave Mikaelian lens fed by line source. (h)–(k) Experimental results of broadband achromatic focusing from 30 to 60 kHz . (l) Comparison between measured FWHM (orange) and simulated FWHM (green).

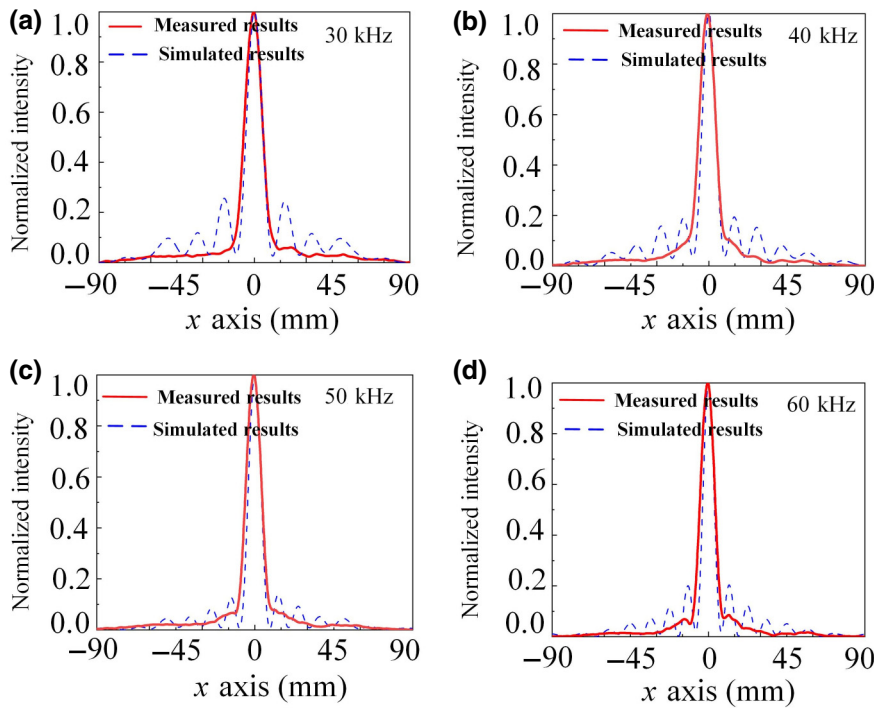


FIG. 5. Comparison between simulated (blue) and measured (red) normalized intensity profiles at the focusing line with frequencies of 30, 40, 50, and 60 kHz.

in Fig. 4(I), achromatic subwavelength focusing is apparently observed. Although the measured FWHM is slightly larger than that of the simulated one in general, considering the testing error and the machining error, the deviation between the measured FWHM and that of the simulated one is negligible. To quantitatively make a further comparison between the measured results and those simulated, the normalized intensity profiles at the focusing line are presented in Fig. 5. Except for the suppression of side lobes, the measured results are in good agreement with those simulated. To quantitatively evaluate the focusing efficiency, the normalized energy intensity of the transmitted field (the square of the displacement amplitude) to that of the incident field is adopted by us [55]. The derived results from experimental data imply that the wave energy at the focus spot is increased to over 7 times that of the incident waves, which is even better than that of Ref. [55]. Therefore, it can be concluded that excellent subwavelength focusing is accomplished. Furthermore, owing to the good performance of side-lobe suppression, the measured focusing performance is even better than that simulated, and thus, it could be utilized in high-resolution imaging. Therefore, all of our designed Mikaelian lens functions are experimentally validated. The transformation method is successfully applied to design broadband multifunctional flexural-wave devices to manipulate flexural waves.

V. SUMMARY

In this work, a passive multifunctional achromatic Mikaelian lens for flexural waves is proposed based on conformal transformation. The GRIN profile derived

from conformal transformation is realized by variation of the thickness of the thin plate. A conformally mapped Mikaelian lens is presented, fabricated, and experimentally demonstrated. Achromatic subwavelength focusing with a FWHM of around 0.30λ and beam-scanning angle of up to 120° are well accomplished over the frequency ranges from 30–120 and 30–180 kHz, respectively. This implies that this Mikaelian lens has significant potential to be applied in high-resolution medical imaging and flexural-wave communication. This work may stimulate the development of broadband and multifunctional devices to manipulate guided elastic waves in platelike structures.

ACKNOWLEDGMENTS

This work is supported by National Natural Science Foundation of China (Grants No. 11872113 and No. 12172271).

-
- [1] J. B. Pendry, D. Schurig, and D. R. Smith, Controlling electromagnetic fields, *Science* **312**, 1780 (2006).
 - [2] U. Leonhardt, Optical conformal mapping, *Science* **312**, 1777 (2006).
 - [3] D. Schurig, J. J. Mock, B. J. Justice, S. A. Cummer, J. B. Pendry, A. F. Starr, and D. R. Smith, Metamaterial electromagnetic cloak at microwave frequencies, *Science* **314**, 977 (2006).
 - [4] R. Liu, C. Ji, J. J. Mock, J. Y. Chin, T. J. Cui, and D. R. Smith, Broadband ground-plane cloak, *Science* **323**, 5912 (2009).

- [5] J. Valentine, J. Li, T. Zentgraf, G. Bartal, and X. Zhang, An optical cloak made of dielectrics, *Nature Mater.* **8**, 568 (2009).
- [6] Y. Luo, H. S. Chen, J. J. Zhang, L. X. Ran, and J. A. Kong, Design and analytical full-wave validation of the invisibility cloaks, concentrators, and field rotators created with a general class of transformations, *Phys. Rev. B*. **77**, 125127 (2008).
- [7] H. Y. Chen, C. T. Chan, and P. Sheng, Transformation optics and metamaterials, *Nat. Mater.* **9**, 387 (2010).
- [8] L. Xu and H. Y. Chen, Transformation metamaterials, *Adv. Mater.* **33**, 200589 (2021).
- [9] W. Wang, L. Lin, X. F. Yang, J. H. Cui, C. L. Du, and X. G. Luo, Design of oblate cylindrical perfect lens using coordinate transformation, *Opt. Express*. **16**, 8094 (2008).
- [10] Y. D. Xu, S. W. Du, and H. Y. Chen, Overlapped illusion optics: A perfect lens brings a brighter feature, *New J. Phys.* **13**, 023010 (2011).
- [11] D. Schurig, J. B. Pendry, and D. R. Smith, Transformation-designed optical elements, *Opt. Express* **15**, 14772 (2007).
- [12] S. A. Cummer and D. Schurig, One path to acoustic cloaking, *New J. Phys.* **9**, 45 (2007).
- [13] H. Y. Chen and C. T. Chan, Acoustic cloaking and transformation acoustics, *J. Phys. D* **43**, 113001 (2010).
- [14] H. Y. Chen and C. T. Chan, Acoustic cloaking in three dimensions using acoustic metamaterials, *Appl. Phys. Lett.* **91**, 183518 (2007).
- [15] L. Zigoneanu, B.-L. Popa, and S. A. Cummer, Three-dimensional broadband omnidirectional acoustic ground cloak, *Nat. Mater.* **13**, 352 (2010).
- [16] S. Zhang, C. G. Xia, and N. Fang, Broadband Acoustic Cloak for Ultrasound Waves, *Phys. Rev. Lett.* **106**, 024301 (2011).
- [17] Y. Chen, M. Y. Zheng, X. N. Liu, Y. F. Bi, Z. Y. Sun, P. Xiang, J. Yang, and G. K. Hu, Cloaking of matter waves, *Phys. Rev. B*. **95**, 180104 (2017).
- [18] J. Zhu, Yongquan Liu, Zixian Liang, Tianning Chen, and Jensen Li, Elastic Waves in Curved Space: Mimicking a Wormhole, *Phys. Rev. Lett.* **121**, 234301 (2018).
- [19] N. Stenger, M. Wilhelm, and M. Wegener, Experiments on Elastic Cloaking in Thin Plates, *Phys. Rev. Lett.* **108**, 014301 (2012).
- [20] D. J. Colquitt, M. Brun, M. Gei, A. B. Movchan, N. V. Movchan, and I. S. Jones, Transformation elastodynamics and cloaking for flexural waves, *J. Mech. Phys. Solids*. **72**, 131 (2014).
- [21] C. Y. Li, L. Xu, L. L. Zhu, S. Y. Zou, Q. H. Liu, Z. Y. Wang, and H. Y. Chen, Concentrators for Water Waves, *Phys. Rev. Lett* **121**, 104501 (2018).
- [22] S. Zhang, D. A. Genov, C. Sun, and X. Zhang, Cloaking of Matter Waves, *Phys. Rev. Lett.* **100**, 123002 (2008).
- [23] N. Yu, P. Genevet, M. A. Kats, F. Aieta, J. P. Tetienne, F. Capasso, and Z. Gaburro, Light propagation with phase discontinuities: Generalized laws of reflection and refraction, *Science* **334**, 333 (2011).
- [24] Y. Xie, W. Wang, H. Chen, A. Konneker, B. I. Popa, and S. A. Cummer, Wavefront modulation and subwavelength diffractive acoustics with an acoustic metasurface, *Nat. Commun.* **5**, 5553 (2014).
- [25] Y. Liu, Z. Liang, F. Liu, O. Diba, A. Lamb, and J. Li, Source Illusion Devices for Flexural Lamb Waves Using Elastic Metasurfaces, *Phys. Rev. Lett.* **119**, 034301 (2017).
- [26] J. Zhang, X. Zhang, F. Xu, X. Ding, M. Deng, N. Hu, and C. Zhang, Vibration control of flexural waves in thin plates by 3D-printed metasurfaces, *J. Sound Vib.* **481**, 115440 (2020).
- [27] J. Zhang, Y. Tian, Y. Cheng, and X. Liu, Acoustic holography using composite metasurfaces, *Appl. Phys. Lett.* **116**, 030501 (2020).
- [28] S.-W. Fan, S.-D. Zhao, L. Cao, Y. Zhu, A. L. Chen, Y.-F. Wang, K. Donda, Y.-S. Wang, and B. Assouar, Reconfigurable curved metasurface for acoustic cloaking and illusion, *Phys. Rev. B* **101**, 024104 (2020).
- [29] H. Zhu, T. F. Walsh, and F. Semperlotti, Total-internal-reflection elastic metasurfaces: Design and application to structural vibration isolation, *Appl. Phys. Lett.* **113**, 221903 (2018).
- [30] L. Cao, Z. Yang, Y. Xu, S.-W. Fan, Y. Zhu, Z. Chen, Y. Li, and B. Assouar, Flexural wave absorption by lossy gradient elastic metasurface, *J. Mech. Phys. Solids* **143**, 104052 (2020).
- [31] P. Wang, F. Casadei, S. Shan, J. C. Weaver, and K. Bertoldi, Harnessing Buckling to Design Tunable Locally Resonant Acoustic Metamaterials, *Phys. Rev. Lett.* **113**, 014301 (2014).
- [32] S. Babaei, N. Viard, P. Wang, N. X. Fang, and K. Bertoldi, Harnessing deformation to switch on and off the propagation of sound, *Adv. Mater.* **28**, 1631 (2016).
- [33] O. R. Bilal, A. Foehr, and C. Daraio, Reprogrammable phononic metasurfaces, *Adv. Mater.* **29**, 1700628 (2017).
- [34] Z. Hou and B. M. Assouar, Tunable solid acoustic metamaterial with negative elastic modulus, *Appl. Phys. Lett.* **106**, 251901 (2015).
- [35] G. Memoli, M. Caleap, M. Asakawa, D. R. Sahoo, B. W. Drinkwater, and S. Subramanian, Metamaterial bricks and quantization of meta-surfaces, *Nat. Commun.* **8**, 14608 (2017).
- [36] Z. Tian, C. Shen, J. Li, E. Reit, Y. Gu, H. Fu, S. A. Cummer, and T. J. Huang, Programmable acoustic metasurfaces, *Adv. Funct. Mater.* **29**, 1808489 (2019).
- [37] S. Li, J. Xu, and J. Tang, Tunable modulation of refracted lamb wave front facilitated by adaptive elastic metasurfaces, *Appl. Phys. Lett.* **112**, 021903 (2018).
- [38] Y. Chen, X. Li, H. Nassar, G. Hu, and G. Huang, A programmable metasurface for real time control of broadband elastic rays, *Smart Mater. Struct.* **27**, 115011 (2018).
- [39] M. Qiu, M. Jia, S. Ma, S. Sun, Q. He, and L. Zhou, Angular Dispersions in Terahertz Metasurfaces: Physics and Applications, *Phys. Rev. Appl.* **9**, 054050 (2018).
- [40] O. Avayu, E. Almeida, Y. Prior, and T. Ellenbogen, Composite functional metasurfaces for multispectral achromatic optics, *Nat. Commun.* **8**, 14992 (2017).
- [41] S. Liu, T. J. Cui, Q. Xu, D. Bao, L. Du, X. Wan, W. X. Tang, C. Ouyang, X. Y. Zhou, H. Yuan, H. F. Ma, W. X. Jiang, J. Han, W. Zhang, and Q. Cheng, Anisotropic coding metamaterials and their powerful manipulation of differently polarized terahertz waves, *Light: Sci. Appl.* **5**, 16076 (2016).

- [42] D. Wen, F. Yue, G. Li, G. Zheng, K. Chan, S. Chen, M. Chen, K. F. Li, P. W. Wong, K. W. Cheah, E. Y. Pun, S. Zhang, and X. Chen, Helicity multiplexed broadband metasurface holograms, *Nat. Commun.* **6**, 8241 (2015).
- [43] A. Darabi and M. J. Leamy, Tunable Nonlinear Topological Insulator for Acoustic Waves, *Phys. Rev. Appl.* **12**, 044030 (2019).
- [44] J. J. Rong, W. J. Ye, S. Y. Zhang, and Y. J. Liu, Frequency-coded passive multifunctional elastic metasurfaces, *Adv. Funct. Mater.* **30**, 2005285 (2020).
- [45] K. F. Graff, *Wave Motion in Elastic Solids* (Courier Corporation, 2012).
- [46] L. Xu and H. Y. Chen, Conformal transformation optics, *Nat. Photonics* **9**, 15 (2015).
- [47] X. Y. Wang, H. Y. Chen, H. Liu, L. Xu, C. Sheng, and S. N. Zhu, Self-Focusing and the Talbot Effect in Conformal Transformation Optics, *Phys. Rev. Lett.* **119**, 033902 (2017).
- [48] J. Chen, H. C. Chu, Y. Lai, H. Y. Chen, M. J. Chen, and D. N. Fang, Conformally mapped Mikaelian lens for broadband achromatic high resolution focusing, *Laser Photonics Rev.* **15**, 200564 (2021).
- [49] H. Gao, X. S. Fang, Z. M. Gu, T. Liu, S. J. Liang, Y. Li, and J. Zhu, Conformally mapped multifunctional acoustic metamaterial lens for spectral sound guiding and Talbot effect, *Research* **2019**, 1748537 (2019).
- [50] U. Leonhardt, Broadband invisibility by non-Euclidean cloak, *Science* **312**, 1777 (2006).
- [51] Z. Nehari, *Conformal Mapping* (McGraw-Hill Book Company, Inc., New York, MR, 1952), Vol. 13, p. 640.
- [52] A. Climente, D. Torrent, and J. Sánchez-Dehesa, Gradient index lenses for flexural waves based on thickness variations, *Appl. Phys. Lett.* **105**, 064101 (2014).
- [53] W. Huang, H. Ji, J. Qiu, and L. Cheng, Analysis of ray trajectories of flexural waves propagating over generalized acoustic black hole indentations, *J. Sound Vib.* **417**, 216 (2018).
- [54] J. Deng, L. Zheng, and O. Guasch, Elliptical acoustic black holes for flexural wave lensing in plates, *Appl. Acoust.* **174**, 107744 (2021).
- [55] M. Jiang, H.-T. Zhou, X.-S. Li, W.-X. Fu, Y.-F. Wang, and Y.-S. Wang, Extreme transmission of elastic metasurface for deep subwavelength focusing, *Acta Mech. Sin.* **38**, 121497 (2022).